Effect of Viscoelasticity on the Analysis of Single-Molecule Force Spectroscopy on Live Cells

V. K. Gupta,[†] K. B. Neeves,[‡] and C. D. Eggleton[†]

[†]University of Maryland Baltimore County, Baltimore, Maryland; and [‡]Colorado School of Mines, Golden, Colorado

SUPPORTING METHOD

Micromechanical Model of Detachment of Inelastic PMN Cells

If the two cells in Fig. 1 are modeled as solid spheres we can rewrite Eq. (1) for time varying bond stretch by utilizing Newton's second law of motion:

$$a\frac{d^2x}{dt^2} = F(t) - cx(t) - b\frac{dx}{dt}, \tag{1}$$

where *x(t)* is the bond stretch and the parameters *a, b, c* depend on the nature of microvilli. For solid microvilli $a = \rho\frac{4}{3}\pi R^3$, $b = 6\pi\mu R$, and $c = \sigma$. When the microvilli are deformable (viscoelastic) they can be extended and may form a tether when the force is greater than 45 pN [1]. In the extension regime $a = \left(1+\frac{\sigma}{\sigma_m}\right)\rho\frac{4}{3}\pi R^3$, $b = \left(1+\frac{\sigma}{\sigma_m}\right)6\pi\mu R$, and $c = \sigma$, while in the tether regime $a = \rho\frac{4}{3}\pi R^3$, $b = \frac{\sigma}{\mu_m}\rho\frac{4}{3}\pi R^3 + 6\pi\mu R$, and $c = \sigma + \frac{\sigma}{\mu_m}6\pi\mu R$, where σ_m microvillus spring constant and μ_m is effective viscosity of tether (see Table 1). For $F = R_f t$, the solution to Eq. 1 is

$$x(t) = c_1\exp(\alpha t) + c_2\exp(\beta t) + \frac{R_f}{c}\left(t - \frac{b}{c}\right), \tag{2}$$

where

$$\alpha = \frac{-b+\sqrt{b^2-4ac}}{2a}, \beta = \frac{-b-\sqrt{b^2-4ac}}{2a}, \tag{3}$$

and c_1; c_2 are constants of integration that can be determined using the initial conditions x(0) = x'(0) = 0.

We simulate bond formation and rupture utilizing the Dembo model. Using the Dembo model Jadhav et al. [2] successfully demonstrated that the rolling of more compliant cells is relatively smoother and slower compared to cells with stiffer membranes [2], in agreement with the experimental studies performed by Park et al. [3]. Hence, the Dembo model is capable of successfully reproducing the experimentally observed phenomenon. According to this model the force dependent on-rate, k_f, and the off-rate, k_r, are given by [4]

$$k_f = {k_f}^0\exp\left[-\frac{\sigma_{ts}{F_b}^2}{2k_bT\sigma^2}\right],\ k_r = {k_r}^0\exp\left[\frac{\psi(\sigma){F_b}^2}{\sigma^2}\right], \tag{4}$$

where k^0_f and k^0_r are the on-rate and off-rate at an equilibrium distance λ, T is the absolute temperature, k_b is the Boltzmann constant, σ is the bond spring constant, σ_{ts} is the spring constant in the transition state, $F_b = \sigma x(t)$ is the force acting on the bond, and $\psi(\sigma) = \frac{(\sigma - \sigma_{ts})}{2k_bT}$.

Besides the Dembo model there are the Bell and Two-pathway models to simulate bond formation and rupture. According to the Bell model the force dependent on-rate, k_f,, and off-rate, k_r, are given by [5]

$$k_f = k_f{}^0 \exp\left[\frac{F_b(x_\beta - 0.5x)}{k_bT}\right],\ k_r = k_r{}^0 \exp\left(\frac{x_\beta F_b}{k_BT}\right), \quad (5)$$

where x_β is the reactive compliance, k_bT is the thermal energy, x is the bond stretch, and $F_b = \sigma x$ is the force acting on the bond. For L-selectin-PSGL-1 bond the Bell model parameters are x_β = 0.16Å, k^0_r = 8.6 s^{-1} [6].

Evans and co-workers [7] developed the two-state model for bond dissociation from a series of dynamic force spectroscopy (DFS) experiments to characterize the catch-slip transition for the P selectin-PSGL-1 bond. According to this model there are two pathways for dissociation: pathway 1 is very fast and dominates at low forces, while pathway 2 is slower and dominates at high forces. Evans and co-workers [7] proposed that the pathways come from two possible bound states. Bond dissociation via pathway 1 occurs at a constant off-rate k1rup. For the pathway 2, on the other hand, bond dissociation occurs with off rate $k_{2rup} = k^0_2 exp(f/f_\beta)$. The occupancy ratio of these two states dictates the dominant dissociation pathway. The states were assumed to be in equilibrium at all times (fast equilibrium) with a small difference in energy between the state 2 and the state 1 ($\Delta E21$). This energy difference determines the equilibrium occupancy ratio, Φ_0, of state 1 to state 2 at zero force. However, force applied to the bond results a shift in the energy of each state, leading to a change in the energy difference between these states. Then the occupancy ratio of these two states changes exponentially with applied force with a scale of f_{12}. Thus, although pathway 1 may dominate at low forces where equilibrium favors occupancy of state 1, at higher forces, pathway 2 dominates as equilibrium shifts to favor occupancy of state 2. For a bond with this type of catch-slip behavior, the off- rate is given by

$$k_r = \frac{\phi_0 k_{1rup} + \exp\left(\frac{f}{f_{12}}\right)\left[k_2^0 \exp\left(\frac{f}{f_\beta}\right)\right]}{\phi_0 + \exp\left(\frac{f}{f_{12}}\right)}, \quad (7)$$

where f is the force acting on the bond, $\Phi_0 = exp\ (\Delta E_{21}/k_bT)$, T is the absolute temperature, and k_b is the Boltzmann constant. Though the above model was derived for the P-selectin-PSGL-1 bond, experiments have shown similar catch-slip behavior for a L-selectin-PSGL-1 bond. For L-selectin-PSGL-1 bond the catch-slip parameters are k_{1rup} = 150 s^{-1}, k^0_2 = 5 s^{-1}, f_β= 110 pN, ΔE_{12} = 5 pN.nm, f_{12} = 10 pN [8].

3-D simulation of Adhesion and Detachment of Elastic PMN Cells

The two PMN cells in Fig. 1 are modeled as 3-D deformable capsules each containing a Newtonian fluid of density ρ and viscosity μ suspended in a Newtonian fluid with the same density and viscosity. The adhesion and detachment of two deformable PMN cells suspended in a Newtonian fluid is simulated by simultaneously: 1) solving the Navier-Stokes (N-S) equation by immersed boundary method (IBM) for motion of deformable capsules suspended in a Newtonian fluid (viscosity = 0.8 cP); 2) solving the constitutive equation using the finite element method for the neo-Hookean membrane of the spherical capsule [9]; and 3) simulating the formation and breakage of receptor (PSGL-1)-ligand (L-selectin) bond using Monte Carlo method with kinetic rate constant based on the Hookean spring (Dembo) model [10, 11]. Cell deformability is controlled by varying membrane stiffness *Eh*. The reader is referred to our previous articles [12, 13] for a detailed description of the numerical implementation of the deformable cell model and corresponding parameter values. As soon as a bond between the two PMN cells is formed we apply an equal and opposite force F on the surface of each cell along the line connecting their centers causing bond stretching and eventually bond rupture (see Fig. 1).

Model and Computational Parameters

We simulated adhesion and detachment of two PMN cells using the parameter values listed in Table 1 unless stated otherwise. All the results presented in this work are obtained using the Dembo model unless stated otherwise. The simulated values for unstressed off-rate and spring constant are 3 s^{-1} and 4 dyn/cm, respectively. The center to center distance between the two cells is 8:25 μm. A time step of 10^{-7} s is used in all these simulations. For inelastic cell model the bond rupture force data sets are generated from Eq. (2) utilizing the relevant model parameters listed in Table 1. In this case cell membrane elasticity is not a relevant parameter. On the other hand for elastic cell model the cell membrane elasticity is controlled by varying membrane stiffness Eh. For our elastic cell model two 3-D deformable stress-free capsules representing two PMN cells are placed in the 3-D fluid computational domain of a box of size 8R×8R×8R. Using the 3D-IBM we calculated the loading history on bonds attached to deformable cells at various loading rates [12, 13]. Then, we conducted 10^5 Monte Carlo simulations in which we imposed the loading history for a deformable cell at a given loading rate on the bond to get statistically accurate histograms for rupture force and bond stretch. In both inelastic and elastic cell models when microvilli are modeled deformable (viscoelastic) then their extension and tether formation are controlled by the microvillus spring constant (σ_m) and the effective viscosity of tether (μ_m), respectively. The initial van der Waals attraction between a pair of microvillus separated by 0.05 μm is approximately 0:001 pN (see Eq. A9 in [10]), which is very small compared to the tensile load on a microvillus; hence, we do not consider van der Waals attraction in our model simulation. Similarly, the electrostatic and steric stabilization forces have been neglected because these forces exist in biological systems at distances from 50 to 250 Å [10].

SUPPORTING REFERENCES

[1] Shao, J.Y., H.P. Ting-Beall, and R.M. Hochmuth. 1998. Static and dynamic lengths of neutrophil microvilli. Proc. Natl. Acad. Sci. USA. 95:6797-6802.

[2] Jadhav, S., C.D. Eggleton, and K. Konstantopoulos. 2005. A 3-D computational model predicts that cell deformation affects selectin-mediated leukocyte rolling. Biophys. J. 88:96-104.

[3] Park, E.Y., M.J. Smith, E.S. Stropp, K.PR. Snapp, J.A. Divietro, W.F. Walker, D.W. Schmidtke, S.L. Diamond, and M.B. Lawrence. 2002. Comparison of PSGL-1 microbead and neutrophil rolling: microvillus elongation stabilizes P-selectin bond clusters. Biophys. J. 82:1835-1847.
[4] Dembo, M., D. C. Torney, K. Saxman, and D. Hammer. 1988. The reaction-limited kinetics of membrane-to-surface adhesion and detachment. Proc. R. Soc. Lond. B. 234:55-83.
[5] Bell, G.I. 1978. Models for the specific adhesion of cells to cells. Science 200:618-627.
[6] Chang, K.-C., D.F.J. Tees, and D.A. Hammer. 2000. The state diagram on cell adhesion under ow: Leukocyte rolling and firm adhesion. Proc. Natl. Acad. Sci. 97(21):11262-11267.
[7] Evans, E., A. Leung, V. Heinrich, and C. Zhu. 2004. Mechanical switching and coupling between two dissociation pathways in a P-selectin adhesion bond. Proc. Natl. Acad. Sci. USA. 101:11281-11286
[8] Caputo, K.E., D. Lee, M.R. King, and D.A. Hammer. 2007. Adhesive dynamics simulations of the shear threshold effect for leukocytes. Biophys. J. 92:787-797.
[9] Eggleton, C.D., A.S. Popel. 1998. Large deformation of red blood cell ghosts in a simple shear flow. Physics of Fluids 10:1834-1845.
[10] Hammer, D.A., and S.M. Apte. 1992. Simulation of cell rolling and adhesion on surfaces in shear flow: general results and analysis of selectin-mediated neutrophil adhesion. Biophys. J. 63:35-57.
[11] Dembo, M. 1994. On peeling an adherent cell from a surface. In Vol. 24 of series: Lectures on Mathematics in the Life Sciences, Some Mathematical Problems in Biology. American Mathematical Society, Providence, RI. 51-77.
[12] Gupta, V.K., I. A. Sraj, K. Konstantopoulos, C. D. Eggleton. 2010. Multi-scale simulation of L-selectin_PSGL-1-dependent homotypic leukocyte binding and rupture. Biomechan. Model. Mechanobiol. 9(5):613-627.
[13] Gupta, V.K., and C.D. Eggleton. 2011. Effect of cell and microvillus mechanics on the transmission of applied loads to single bonds in dynamic force spectroscopy. Phys. Rev. E. 84:011912.

Supplementary Figure Captions

Figure S1. Time variation of applied force (solid line), intermolecular bond force with solid microvillus (dashed line) and intermolecular bond force with deformable microvillus (dashed dot line) obtained from micromechanical model simulation at (a) $R_f = 10^3$ pN/s, (b) $R_f = 10^4$ pN/s, (c) $R_f = 10^5$ pN/s, (d) $R_f = 10^6$ pN/s, (e) $R_f = 10^7$ pN/s. Corresponding data marked with red is obtained from 3-D IBM simulation of deformable cell for the model parameters listed in Table 1.

Figure S2. Effect of time step (Δt) and grid resolution (N) on the intermolecular bond force for "solid cell with deformable microvillus" and "deformable cell with deformable microvillus" cell models at $R_f = 10^6$ pN/s.

Figure S3. Rupture force histograms based on (a) applied force (b) intermolecular bond force for the legend corresponding to Fig. S1.

Supplementary Figure-1

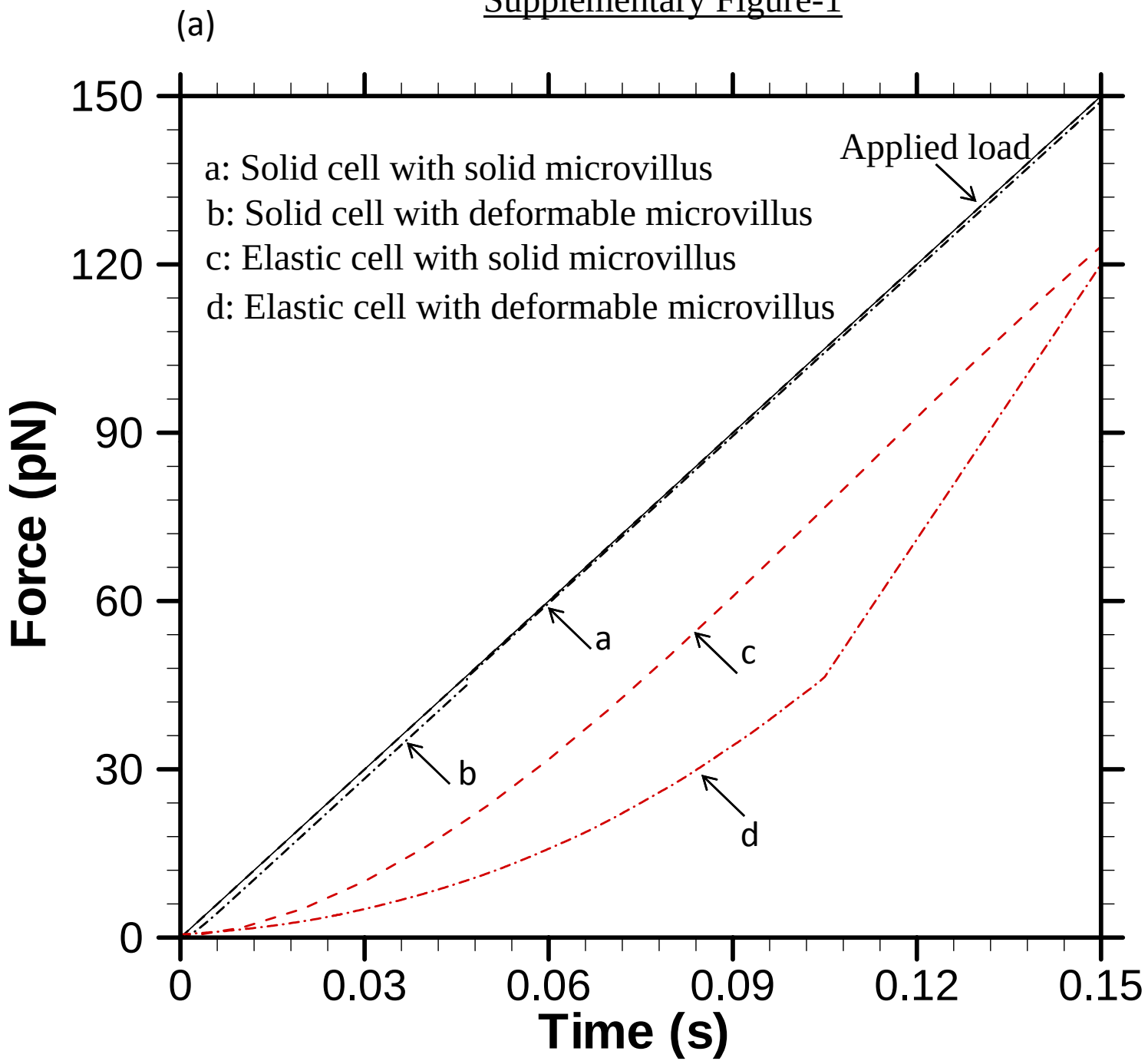

(b) Supplementary Figure-1

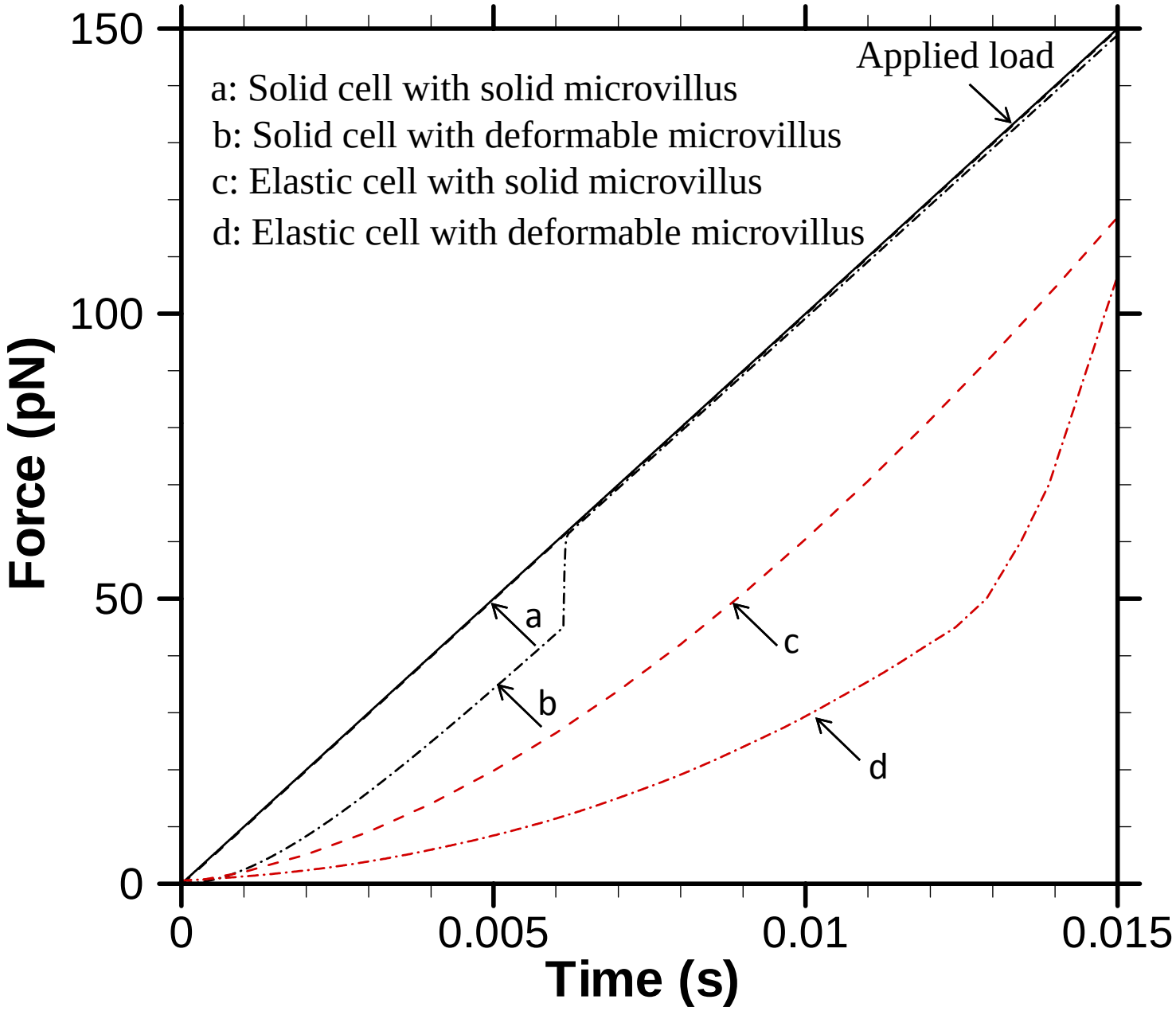

Supplementary Figure-1

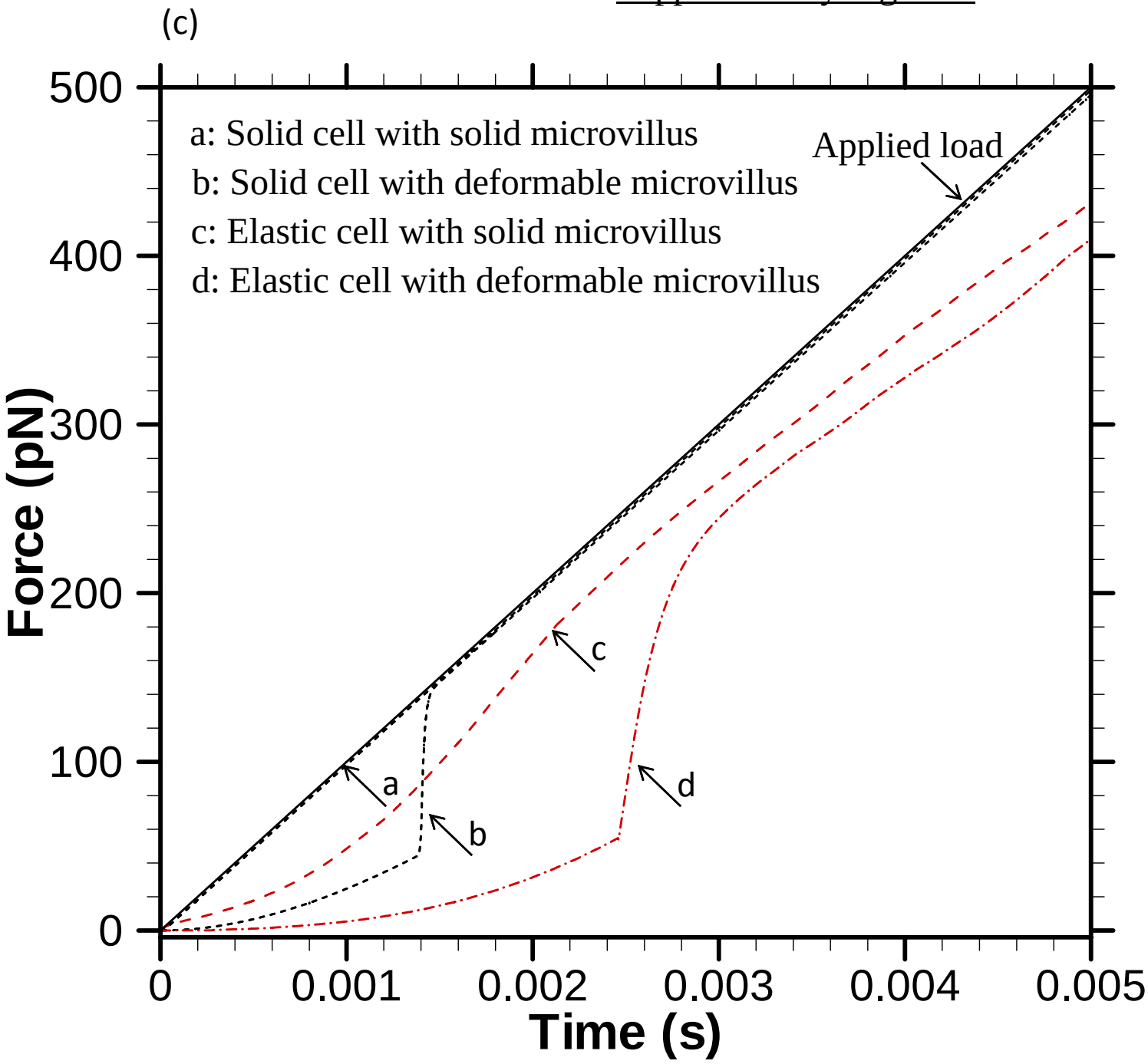

(d)

Supplementary Figure-1

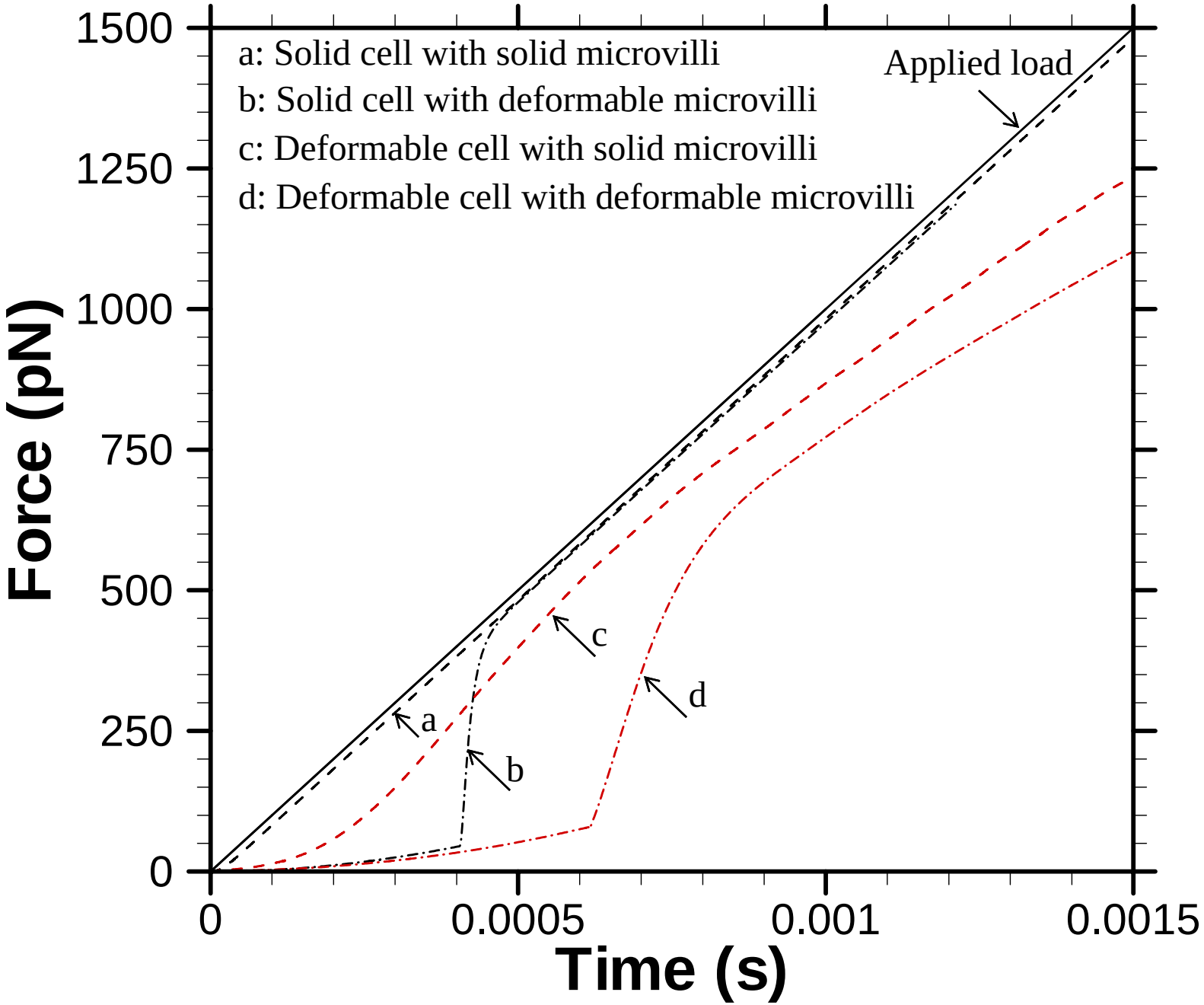

Supplementary Figure-1

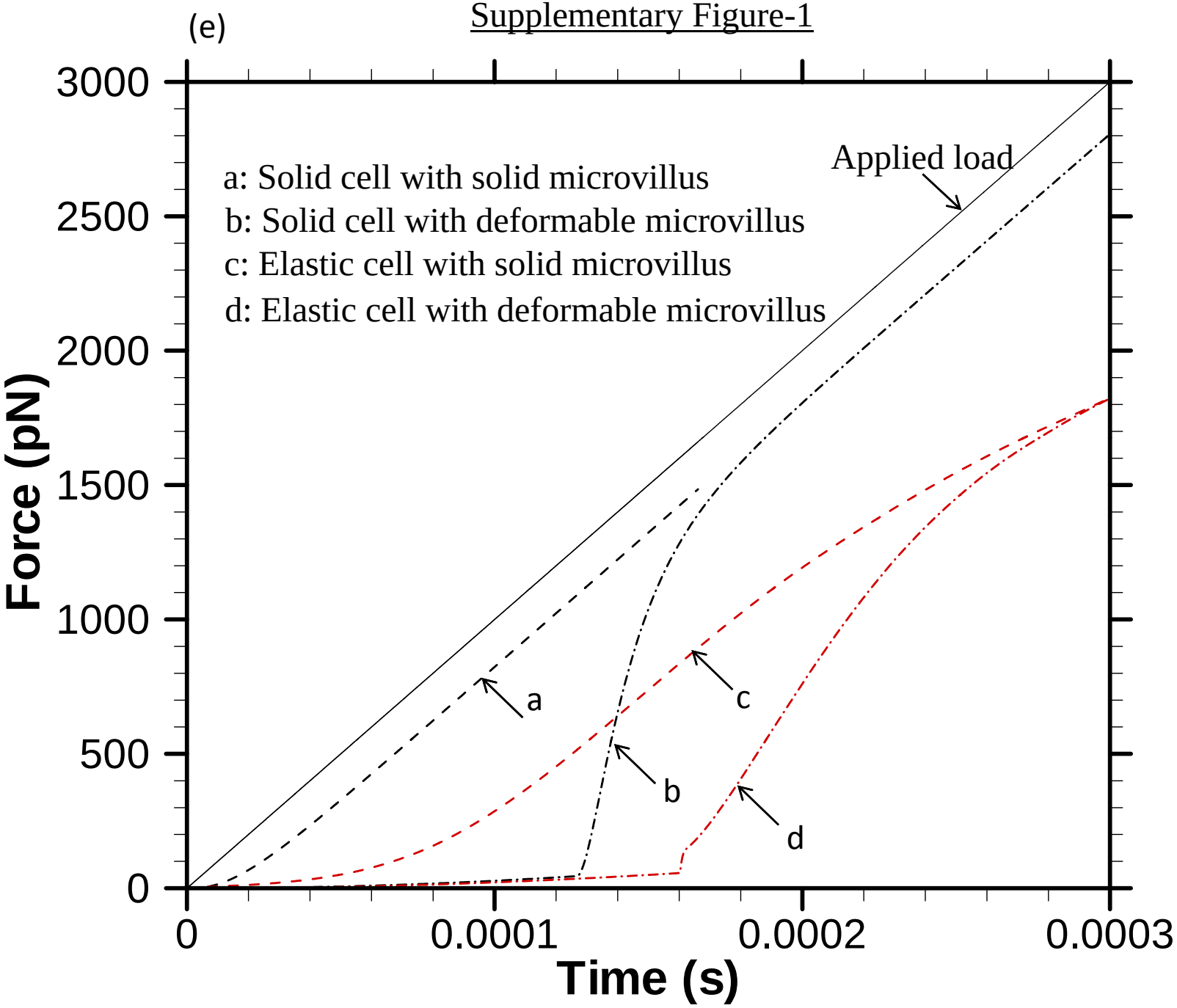

Supplementary Figure-2

(a) Solid cell with deformable microvillus

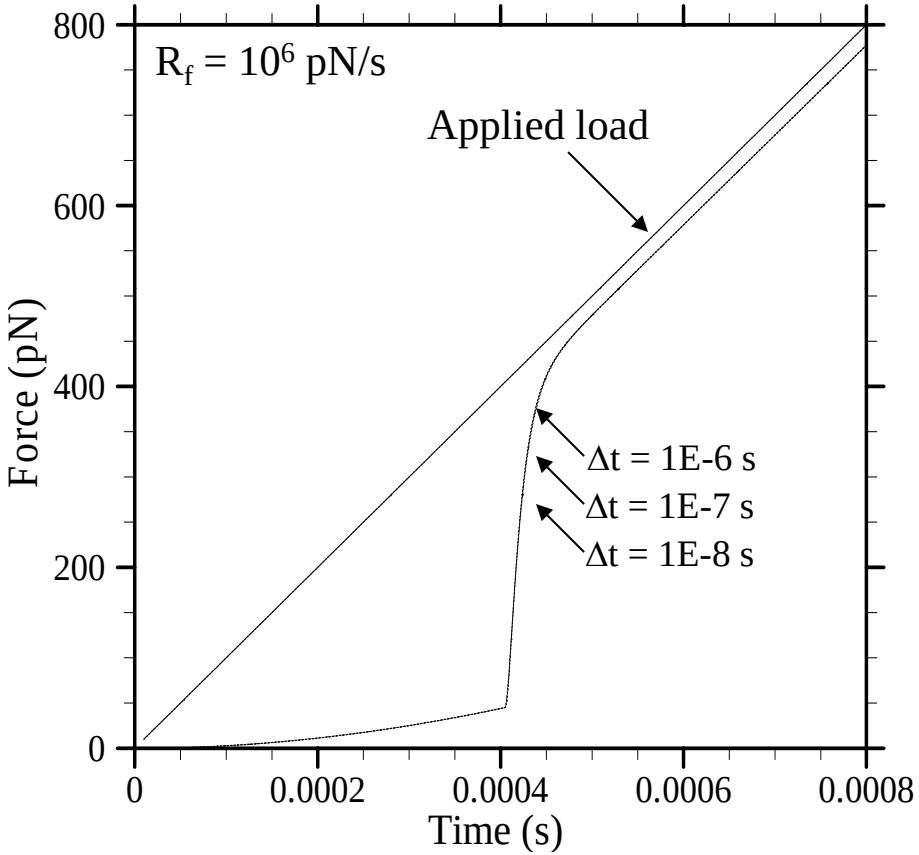

(b) Deformable cell with deformable microvillus

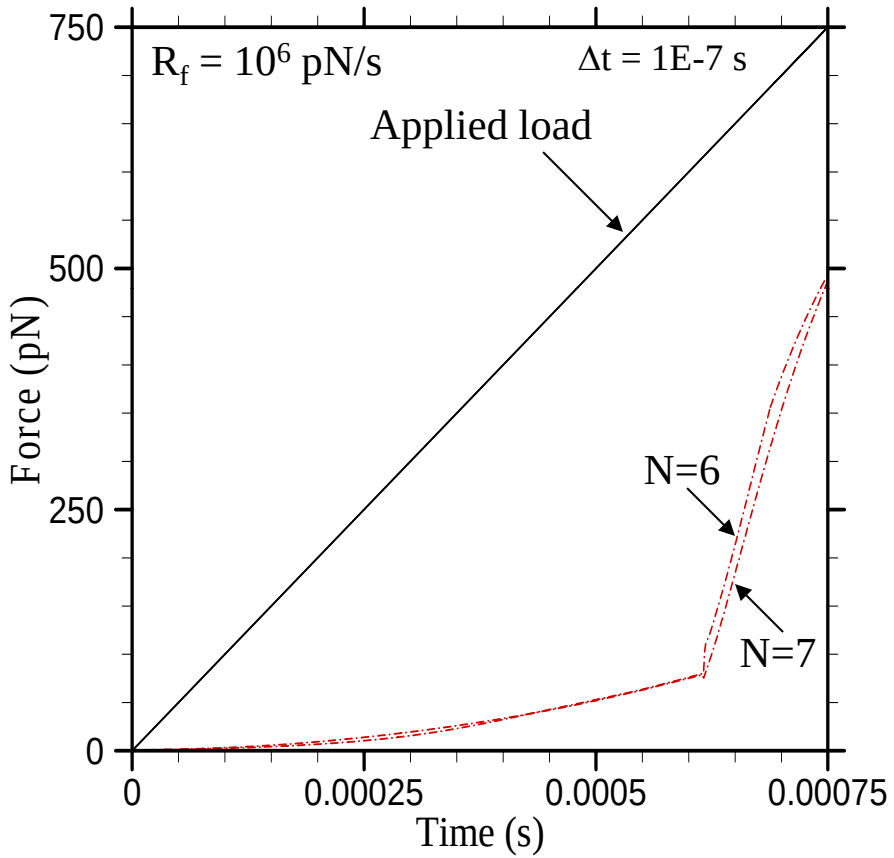

Supplementary Figure-3

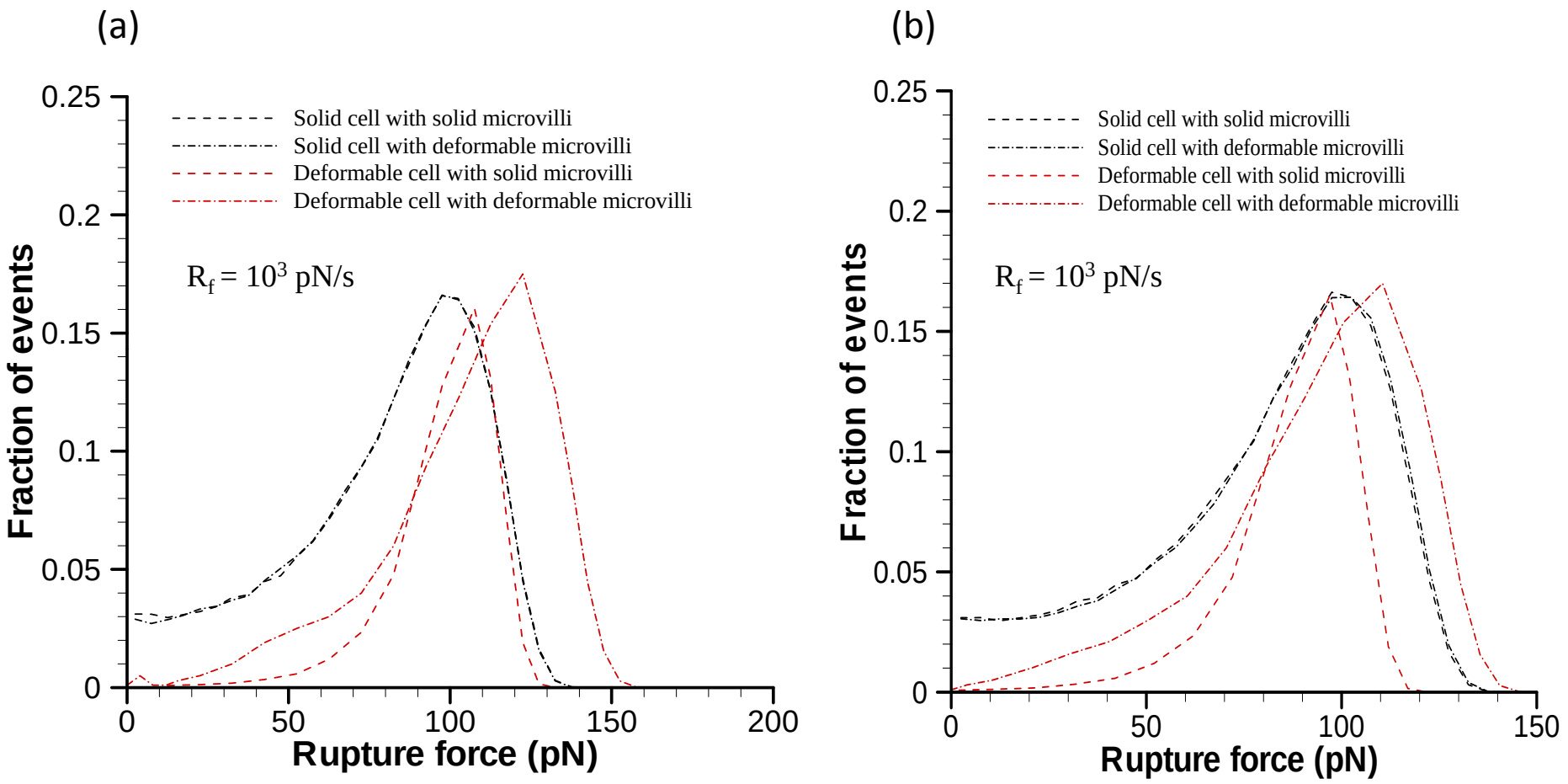

Supplementary Figure-3

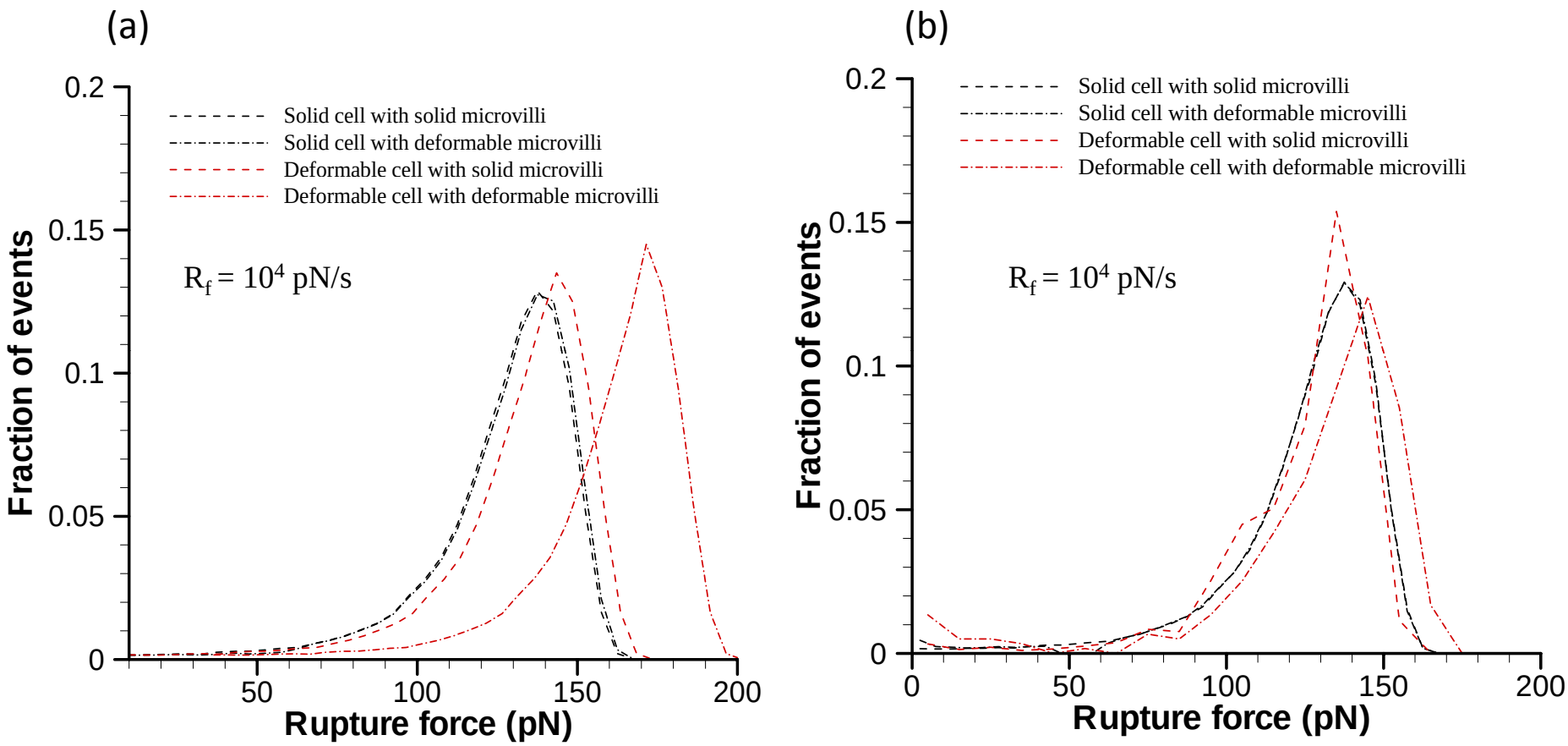

Supplementary Figure-3

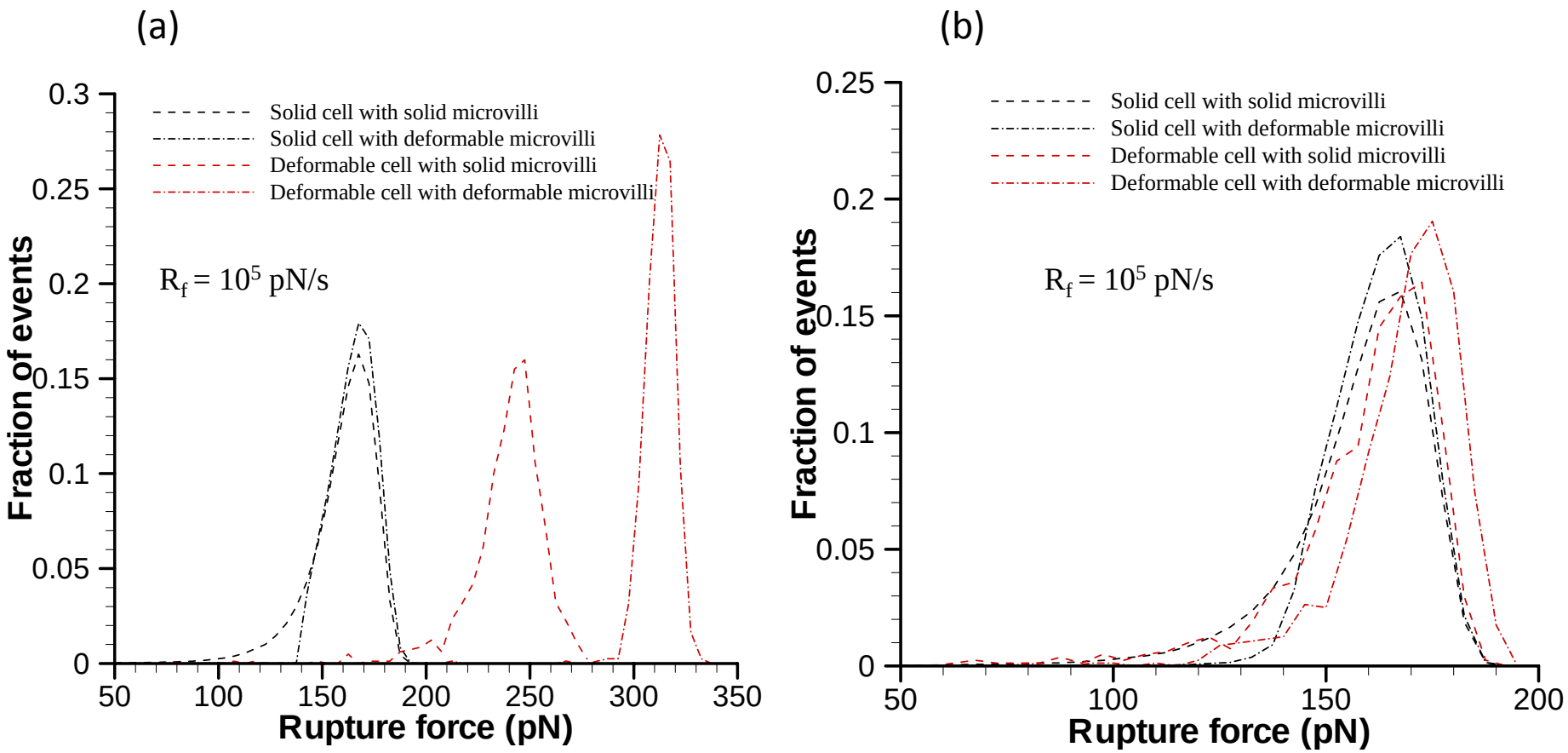

Supplementary Figure-3

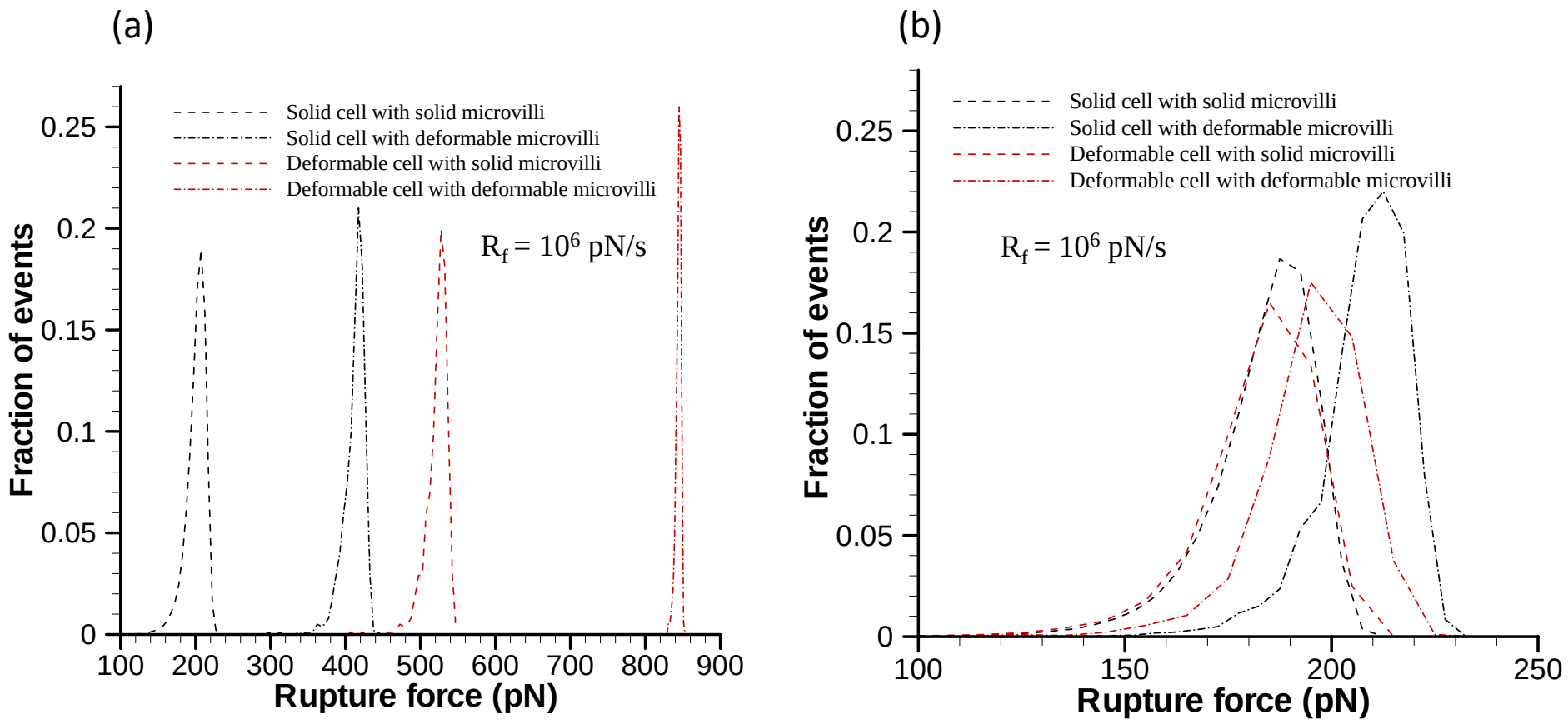

Supplementary Figure-3